

Monte Carlo Simulation of Silicon Nanowire Thermal Conductivity

Yunfei Chen¹

Department of Mechanical Engineering and
China Education Council Key Laboratory of
MEMS, Southeast University, Nanjing, 210096,
People's Republic of China

Deyu Li

Department of Mechanical Engineering,
Vanderbilt University, Nashville, TN, 37235-1592

Jennifer R. Lukes

Department of Mechanical Engineering and
Applied Mechanics, University of Pennsylvania,
Philadelphia, PA 19104-6315

Arun Majumdar

Department of Mechanical Engineering,
University of CA, Berkeley, California, 94720
Materials Science Division, Lawrence Berkeley
National Lab, Berkeley, CA, 94720

Monte Carlo simulation is applied to investigate phonon transport in single crystalline Si nanowires. Phonon-phonon normal (N) and Umklapp (U) scattering processes are modeled with a genetic algorithm to satisfy energy and momentum conservation. The scattering rates of N and U scattering processes are found from first-order perturbation theory. The thermal conductivity of Si nanowires is simulated and good agreement is achieved with recent experimental data. In order to study the confinement effects on phonon transport in nanowires, two different phonon dispersions, one from experimental measurements on bulk Si and the other solved from elastic wave theory, are adopted in the simulation. The discrepancy between simulations using different phonon dispersions increases as the nanowire diameter decreases, which suggests that the confinement effect is significant when the nanowire diameter approaches tens of nanometers. It is found that the U scattering probability in Si nanowires is higher than that in bulk Si due to the decrease of the frequency gap between different modes and the reduced phonon group velocity. Simulation results suggest that the dispersion relation for nanowires obtained from elasticity theory should be used to evaluate nanowire thermal conductivity as the nanowire diameter is reduced to the sub-100 nm scale. [DOI: 10.1115/1.2035114]

Keywords: Nanowire, Monte Carlo Simulation, Thermal Conductivity, Dispersion Relations, Phonon Scattering, Genetic Algorithm

1 Introduction

An accurate numerical prediction of the thermal transport in nanoscale crystalline structures is very important for both fundamental physics and engineering applications. A comprehensive analysis of thermal conductivities of nanostructures can lead to a deeper understanding of phonon scattering mechanisms, which is of fundamental theoretical significance. In addition, aggressive miniaturization of microelectronic devices leads to substantially increased power dissipation. Thermal management is problematic in such devices because at sub-100 nm length scales, thermal conductivity deviates significantly from bulk values and accurate values are often not known. In theoretical analysis of phonon transport, the Boltzmann transport equation (BTE) is often the starting point. Based on the lifetime assumption and with some simplifications, it is possible to achieve a closed form analytical solution of the BTE [1–6]. However, since many assumptions must be introduced to reach a closed form solution, the results may deviate significantly from experimental observations.

In 1966, two numerical techniques were proposed to solve the BTE for electron transport: the Monte Carlo (MC) method [7] and an iterative technique [8]. Since then, MC simulations have found wide application in investigations of electron distribution, average energy, drift velocity, diffusion coefficients, and band structure for carrier transport in semiconductors [9]. In MC simulation, self-consistent calculation must be guaranteed, in which an assumed distribution function $f(k)$ is used to evaluate scattering probabilities and the same $f(k)$ must be obtained as the solution. Since electron-electron interactions do not significantly affect electron transport in semiconductors, they are often neglected in the traditional MC simulation. Several efforts [10–12] to account for electron-electron interactions showed only partial success and these interactions remain a difficult problem to treat. The MC method cannot be directly implemented to solve the BTE for phonon transport since phonon-phonon interactions must be included

in the simulation of phonon transport. Phonon-phonon scattering processes and phonon relaxation times or lifetimes are essential for phonon transport modeling. Only at extremely low temperature, where ballistic transport dominates, is the phonon-phonon interaction unimportant. In 1988, Klitsner et al. [13] applied the MC method to study ballistic phonon transport and found good agreement with a theoretical analysis. Later Peterson [14] simulated phonon transport using a MC method based on the Debye model, in which all phonons were assumed to have the same propagating speed, and interactions between phonons were accounted for by assuming an average lifetime. With these assumptions, heat transfer in a one-dimensional cell array was simulated and the time evolution of the temperature profile was predicted. In 2002, Mazumder and Majumdar [15] reported MC simulation for phonon transport in thin Si films. In their work, phonon polarization and phonon dispersion were taken into account by considering the dependence of phonon lifetime on frequency, polarization, and temperature. Their simulation results agreed well with the experimental data for temperatures lower than room temperature. However, for higher temperature, the three-phonon scattering probability increases and the phonon transition rates between different polarization and different frequency phonons increase. Simple models assuming that the phonon transition process is based on an averaged phonon lifetime lead to unconverged results for phonon transport. Hence for MC simulation at high temperature, self-consistent calculations must be performed to ensure convergence of the simulations.

In the present work, we first modify the MC technique to study phonon transport in bulk Si at temperatures both below and above room temperature (up to 500 K), and then apply the method to model phonon transport in Si nanowires. All important phonon scattering processes in semiconductors, such as three-phonon scattering, boundary scattering, and impurity scattering are taken into account. A genetic algorithm is adopted to guarantee both energy and momentum conservation for normal (N) scattering and energy conservation for Umklapp (U) scattering. The simulation results for the thermal conductivity of bulk Si fit the experimental results very well in the temperature range from 40 K to 500 K. Below 40 K, since no boundary scattering is included in the simulation for

¹Electronic mail: yunfeichen@yahoo.com

Contributed by the Heat Transfer Division of ASME for publication in the JOURNAL OF HEAT TRANSFER. Manuscript received: September 28, 2004; final manuscript received: May 18, 2005. Review conducted by: Gang Chen.

bulk Si, the simulation results deviate from the experimental value. For the thermal conductivity of Si nanowires, the simulation results agree reasonably well with recent experimental results [16,17].

2 Transport Model and Monte Carlo Method

The Boltzmann equation for phonon transport in the presence of a temperature gradient is written as

$$\vec{V}_g \cdot \nabla T \frac{dn}{dT} = \left(\frac{\partial n}{\partial t} \right)_c \quad (1)$$

where \vec{V}_g is the group velocity

$$\vec{V}_g = \nabla_{\vec{q}} \omega \quad (2)$$

n is the distribution function, q is the phonon wave vector, T is the local temperature, ω is the phonon frequency, and $(\partial n / \partial t)_c$ is the rate of change of n due to collisions. On the left side of Eq. (1), n can be replaced by n_0 , the equilibrium Planck distribution. Consequently Eq. (1) can be read as

$$\vec{V}_g \cdot \nabla T \frac{dn_0}{dT} = \sum_{k'} [\Phi(q, q') n(q') - \Phi(q', q) n(q)] \quad (3)$$

where

$$n_0 = \frac{1}{\exp(\hbar \omega / k_B T) - 1} \quad (4)$$

Here \hbar is the Planck's constant divided by 2π , k_B is the Boltzmann's constant, and $\Phi(q, q')$ is the function describing the scattering rate from state q' to state q , which depends on the phonon frequency and polarization.

Equation (3) is a nonlinear integrodifferential equation. The transition rate $\Phi(q, q')$ on the right side of Eq. (3) is very complicated, and without simplification the formulation is difficult to solve. This difficulty can be avoided by using MC. To calculate thermal transport, MC does not try to solve Eq. (3) directly, but instead, follows a large number of phonons in a three-dimensional space subjected to a temperature gradient. The simulation domain is divided into many cells and initial local temperature is imposed on each cell according to the temperature gradient. The initial velocity, polarization, and frequency of each phonon are based on the local temperature. More details on the initial conditions can be found in Ref. [15]. The number of phonons in each cell depends on the local temperature and the cell volume. For silicon, the frequency range between zero and the maximum cut-off frequency of the longitudinal acoustic branch is divided into 1000 spectral intervals. The number of phonons per unit volume in the i th spectral interval is calculated from the equilibrium Planck distribution

$$N_i = \langle n(\omega_{0,i}, LA) \rangle D(\omega_{0,i}, LA) \Delta \omega_i + 2 \langle n(\omega_{0,i}, TA) \rangle D(\omega_{0,i}, TA) \Delta \omega_i \quad (5)$$

where $n(\omega_{0,i}, LA)$ and $n(\omega_{0,i}, TA)$ are the Bose-Einstein distribution for the longitudinal and transverse acoustic branches, respectively. $D(\omega_{0,i})$ is the density of states, and $\Delta \omega = \omega_{\max, LA} / N_b$, in which N_b is the number of intervals from zero to the maximum cutoff frequency of the longitudinal acoustic branch. In Eq. (5), three acoustic branches in the phonon dispersion relation are taken into account, i.e., one longitudinal acoustic branch and two transverse acoustic branches. Optical phonons are not considered because they contribute little to thermal conductivity due to their small group velocity. In this paper N_b is selected to be 1000. The total number of phonons can be obtained by summing up the phonons in the 1000 spectral intervals

$$N = \sum_{i=1}^{N_b} N_i \quad (6)$$

The actual number of phonons per unit volume calculated from Eq. (6) is usually a very large number. With the current computational power, it is impossible to simulate the movements of such a large number of phonons in each cell. In order to save computation time, a prescribed number of phonons are used to represent the actual phonons in each cell by introducing a scaling factor

$$W = \frac{N_{\text{actual}}}{N_{\text{prescribed}}} \quad (7)$$

Equation (7) indicates that one phonon in the simulation code stands for W actual phonons.

Once the phonons are produced, the simulation starts with all of the phonons in given initial conditions with appropriate sampled frequencies, group velocities, wave vectors, and polarizations. A duration of free flight is set and all of the phonons move linearly from initial positions to new positions such that

$$\vec{r}_i = \vec{r}_{0,i} + \vec{V}_{g,i} \Delta t \quad (8)$$

where \vec{r}_i , $\vec{r}_{0,i}$ are the new and initial positions of the i th phonon, respectively, and Δt is the free flight time. The free flight time is kept constant during the simulation and its value is set as small as possible in order to not miss any scattering events. However, smaller Δt increases computation expense. To avoid undue computational burden, the time step in our simulation was set as one half of the smallest phonon scattering time. It was found that this time step gave stable simulation results. If the phonon encounters a boundary during free flight, it is reflected as described in Sec. 3.1. If it does not, the phonon lifetime is calculated according to Matthiessen's rule

$$\frac{1}{\tau_T} = \frac{1}{\tau_i} + \frac{1}{\tau_U} + \frac{1}{\tau_N} \quad (9)$$

where the total phonon lifetime τ_T depends on the lifetime for impurity scattering τ_i , the lifetime for U processes τ_U , and the lifetime for N processes τ_N . Each phonon has its own unique lifetime based on its frequency, polarization, impurity scattering time scale, and local temperature [3]. The calculation of these lifetimes is discussed in more detail in the following sections and in Table 1. $P(t)$, the probability that a phonon has already existed for a free flight time Δt without being scattered, decreases with time such that

$$\frac{\partial P}{\partial t} = -\frac{P}{\tau_T} \quad (10)$$

The probability that the phonon is scattered after the free flight time is

$$\bar{P} = 1 - P = 1 - \exp(-\Delta t / \tau_T) \quad (11)$$

To impose a statistical scattering mechanism on the phonon, a random number R_1 , is generated. If $R_1 < \bar{P}$, the phonon will be scattered and replaced by a new phonon at a different state. Then the new phonon begins its new free flight. If $R_1 > \bar{P}$, the phonon will continue its free flight with its state unchanged. If the simulation time is long enough, the system equilibrates, and the final results can be extracted through averaging over a fixed time step [15].

When $R_1 < \bar{P}$, a scattered phonon is found, then, the following procedure is used to determine which scattering process the phonon engages in. As described in Eq. (9), three scattering processes constitute the transition rate. However, the phonon can only engage in one of them. In order to distinguish which process the phonon engages in, the phonon lifetime is divided into two parts

$$\frac{1}{\tau_T} = \frac{1}{\tau_1} + \frac{1}{\tau_2} \quad (12)$$

where

Table 1 Parameters used in Monte Carlo simulation

Scattering process	Inverse relaxation time	parameter	
Boundary scattering		d	0.5
Impurity scattering	$\tau_i^{-1} = B_i \omega^4$ (s^{-1})	B_i	5.32×10^{-44} (s^3)
Three phonon			
N process			
Transverse	$\tau_N^{-1} = B_{TN} \omega T^4$ (s^{-1})	B_T	9.3×10^{-13} (deg^{-4})
Longitudinal	$\tau_N^{-1} = B_L \omega^2 T^3$ (s^{-1})	B_L	1.0×10^{-30} ($\text{deg}^{-3} s$)
U process			
Transverse	$\tau_{TU}^{-1} = \begin{cases} 0 & (\omega < \omega_{12}) \\ B_{TU} \omega^2 / \sinh(\frac{\hbar \omega}{k_B T}) & (\omega \geq \omega_{12}) \end{cases}$ (s^{-1})	B_{TU}	5.50×10^{-18} (s)
Longitudinal	$\tau_{LU}^{-1} = B_L \omega^2 T^3$ (s^{-1})	B_L	1.0×10^{-30} ($\text{deg}^{-3} s$)

$$\frac{1}{\tau_1} = \frac{1}{\tau_i} \tag{13}$$

and

$$\frac{1}{\tau_2} = \frac{1}{\tau_N} + \frac{1}{\tau_U} \tag{14}$$

The probability that the phonon engages in impurity scattering process can be expressed as

$$P_i = \frac{1/\tau_1}{1/\tau_T} \tag{15}$$

A random number R_2 is generated. If $R_2 < P_i$, the phonon will be scattered by impurities. Otherwise, it engages in three phonon scattering process. The same approach is used to determine if the phonon engages in N or U scattering processes.

3 Scattering Mechanisms and their Realization in MC Simulations

3.1 Boundary Scattering. During phonon transport, the primary phonon scattering processes are phonon-boundary collisions, impurity scattering, and three-phonon inelastic interactions. Boundary collisions play an important role in thermal resistance as the structure size decreases to nanoscale. When a phonon strikes the structure wall, a random number is first drawn. If this random number is less than a prescribed specularly parameter d , the phonon is specularly reflected using the following equation as in Ref. [15]:

$$\vec{s}_r = \vec{s}_i + |\vec{s}_i \cdot \vec{n}| \vec{n} \tag{16}$$

where \vec{s}_i, \vec{s}_r are the direction vectors of the incident and reflected phonons and \vec{n} is the unit surface normal. In this case the phonon incident angle is equal to the reflected angle. If the random number is larger than d , the phonon is reflected diffusely at the surface. Its direction is selected according to the following relation:

$$\vec{s}_r = \sin \theta \cos \varphi \vec{t}_1 + \sin \theta \sin \varphi \vec{t}_2 + \cos \theta \vec{n} \tag{17}$$

where $\varphi = 2\pi R_3$, $\cos \theta = 2R_4 - 1$, R_3, R_4 are random numbers, \vec{t}_1, \vec{t}_2 are unit surface tangents, which must be perpendicular to each other such that

$$\vec{t}_1 \times \vec{t}_2 = \vec{n} \tag{18}$$

If d is set to 1, the boundary is perfectly smooth and all phonons will be specularly reflected. In this case, the boundary scattering process does not contribute to thermal resistance.

3.2 Impurity Scattering. Impurity scattering can be the dominant phonon scattering mechanism at low temperatures. The time scale for scattering by impurities is expressed using a simple model by Vincenti and Kruger [18]

$$\tau_i^{-1} = \alpha \sigma \rho |\vec{V}_g| \tag{19}$$

where α is a constant of the order of unity, ρ is the defect density per unit volume, and σ is the scattering cross section expressed as [19]

$$\sigma = \pi r^2 \left(\frac{\chi^4}{\chi^4 + 1} \right) \tag{20}$$

Here r is the atomic radius of the impurity and $\chi = r|\vec{q}|$, and \vec{q} stands for the phonon wave vector. If only the isotope scattering is taken into account, Eq. (19) can be simplified as

$$\tau_i^{-1} = B_i \omega^4 \tag{21}$$

If a phonon is scattered by an impurity or a defect, its wave vector will be perturbed and its flight direction will be changed. In order to simulate the impurity scattering process, a new wave vector and a new velocity direction will be generated based on the phonon's frequency. The phonon frequency and polarization keep their original values.

3.3 Three-Phonon Scattering. Three-phonon interactions include both normal and Umklapp scattering processes. Peierls [20]

showed that N processes contribute to thermal resistance by transferring momentum from one group of modes, where resistance (R) processes (Umklapp or impurity processes) are weak, to other modes where R processes are strong. This effect is particularly important for point defect scattering, since the scattering probability is strongly frequency dependent. Callaway [2] assumed that N processes relax toward a quasiequilibrium distribution, i.e., one shifted in momentum space, while R processes tend to restore true equilibrium. The shift of the quasiequilibrium distribution is chosen so that N processes conserve momentum in the aggregate. The displaced Planck distribution can be written as [2]

$$n(\vec{\lambda}) = \left[\exp\left(\frac{\hbar\omega - \vec{\lambda}\cdot\vec{q}}{k_B T}\right) \right]^{-1} = n_0 + \frac{\vec{\lambda}\cdot\vec{q}}{k_B T} \frac{e^{\hbar\omega/k_B T}}{(e^{\hbar\omega/k_B T} - 1)^2} \quad (22)$$

where $\vec{\lambda}$ is a constant vector in the direction of the temperature gradient. From Eq. (22) the departure of the phonon occupation number from that at thermal equilibrium for a small vector interval can be written as

$$\begin{aligned} \Delta N &= \iiint_{\Delta q} [n(\vec{\lambda}) - n_0] d^3 q \\ &= \sum_{q_x} \sum_{q_y} \sum_{q_z} [n(\vec{\lambda}) - n_0] \Delta q_x \Delta q_y \Delta q_z \end{aligned} \quad (23)$$

The three-phonon interactions obey the energy conservation and momentum conservation laws

$$\vec{q}_1 + \vec{q}_2 \leftrightarrow \vec{q}_3 \quad (24)$$

$$\vec{q}_1 + \vec{q}_2 \leftrightarrow \vec{q}_3 + \vec{G} \quad (25)$$

$$\omega_1 + \omega_2 = \omega_3 \quad (26)$$

where \vec{G} is the reciprocal lattice vector.

4 Genetic Algorithm for Three-Phonon Scattering

In three-phonon scattering processes, if an initial phonon produces two phonons, both of the two new phonons will be followed. If an initial phonon is absorbed along with another to create a third phonon in the scattering process, the state of one of the initial phonons will be set as the created phonon and the other one will be destroyed by setting its energy as zero. Then all the scattered phonons will be treated by a genetic algorithm to satisfy momentum and energy conservation.

In order to satisfy Eqs. (24)–(26) simultaneously, a genetic algorithm [21] is introduced to determine the “fitness” of an ensemble of phonons. Fitness is an indication of how well the ensemble satisfies momentum and energy conservations and is reflected by two parameters D_1 and D_2 , which are residuals of the wave vector and frequency, respectively

$$\begin{aligned} D_1 &= \frac{\sum_{i=1}^{N_p} q'_{x,i} - \sum_{i=1}^{N_c} q_{x,i}}{\sum_{i=1}^{N_c} q_{x,i}} + \frac{\sum_{i=1}^{N_p} q'_{y,i} - \sum_{i=1}^{N_c} q_{y,i}}{\sum_{i=1}^{N_c} q_{y,i}} \\ &+ \frac{\sum_{i=1}^{N_p} q'_{z,i} - \sum_{i=1}^{N_c} q_{z,i}}{\sum_{i=1}^{N_c} q_{z,i}} \end{aligned} \quad (27)$$

$$D_2 = \left(\sum_{i=1}^{N_p} \omega'_i - \sum_{i=1}^{N_c} \omega_i \right) / \left(\sum_{i=1}^{N_c} \omega_i \right) \quad (28)$$

Here N_c is the number of phonons involved in a scattering event, $q'_{x,i}$, $q'_{y,i}$, $q'_{z,i}$, ω'_i are the new phonon wave vectors along the x , y , z directions and frequencies, $q_{x,i}$, $q_{y,i}$, $q_{z,i}$, ω_i are the corresponding phonon parameters before scattering. N_p is the number of phonons to be created. In the simulation, the initial value of N_p is set to equal N_c to simplify the optimization process. However, because of the three-phonon scattering process, the total number of phonons may change and it is possible that N_p does not equal N_c . The genetic algorithm operates as follows:

1. Initialization: Create a father generation $F = \{f_j | j=1, \dots, n\}$ of phonon ensembles according to local temperature. Each ensemble f_j is defined as $f_j = \{p_i | i=1, \dots, N_c\}$, so there are N_c phonons per ensemble. Each individual phonon p_i is coded as a 12 digit binary number, so the total number of digits in f_j is $12N_c$. The first digit of each p_i represents the phonon polarization, with 1 standing for LA and 0 for TA. The second digit is a placeholder only, and is always set to 0. The remaining ten digits represent the average phonon frequency. This frequency is the average value in each of the 1000 spectral intervals described above. For example, if a phonon frequency falls in the 600th interval and its polarization is LA, its average frequency is $\omega_{600} = 600/1000 \times \omega_{\max, LA}$ and it is coded as $p_i = [1010 \ 0101 \ 1000]$. It can be seen that the last ten digits represent the value of 600 in binary notation.
2. Reproduction: Create an offspring generation from the father generation using the crossover operation. In this operation, two ensembles from the father generation are randomly selected and some digits (out of the total $12N_c$ digits for each ensemble) are also randomly selected. One offspring ensemble s_i is produced from the first selected father ensemble by exchanging the selected digits with the second selected father ensemble. For example if f_1 and f_2 are the first and second randomly selected ensembles from the father generation as

$$\begin{cases} f_1 = [0, 0, 1, 0, \dots, 1, \underline{1}, 0, \underline{1}] \\ f_2 = [1, 0, 1, 0, \dots, 0, \underline{0}, \underline{0}, 1] \end{cases}$$

and the underlined digits represent the randomly selected digits, the offspring ensemble is generated as $s_i = [0, 0, 1, 0, \dots, 1, 0, 0, 1]$. The number of crossover operations performed, m , is also selected randomly, yielding an offspring ensemble set $S = \{s_1, s_2, \dots, s_m\}$.

3. Initial evaluation: Evaluate all ensembles in F and S and use Eqs. (27) and (28) to calculate the residuals D_1 and D_2 for each ensemble.
4. Selection: Choose the best ensemble from the union of F and S : $f_{\text{best}} \in F \cup S$ by selecting the ensemble with minimum D_1 and D_2 .
5. Mutation: From the best ensemble generate a set of $l/2$ mutants: $M = \{s'_i := \text{mut}(s_{\text{best}}) | i=1, 2, \dots, l/2\}$. The selection of l is arbitrary; in this paper, it is set as six, which means three ensembles will be produced from the best ensemble through the mutation operation. Mutation means that selected digits become 0 if their initial values are 1, and vice versa. For example, if $s_i = [0, 0, 1, 0, \dots, \underline{1}, \underline{1}, 0, 0]$, after the mutation operation, $s'_i = [0, 0, 1, 0, \dots, 0, 0, 1, 0]$ will be produced as one ensemble of the mutant set. k digits are randomly selected in each ensemble to mutate. If k is set too large, it will take a long time for the system to converge due to the algorithm oscillation. The best value of k is set as two or three for the algorithm to be stable. In our simulation k is set to be three.
6. Create a new father generation: Calculate the residuals of all ensembles in M , S , and F , select the na ensembles with the lowest residuals, and create a new father generation F from these. The number na depends on the total number of en-

sembles. If na is set too large, it takes a long time for the genetic algorithm to converge. In this paper, it is set as two in each generation step.

7. Terminate check: If at least one of the ensembles has achieved a predefined fitness, stop and return the best individual. Otherwise, continue with the reproduction step (step 2).

N -type scattering processes should satisfy both momentum and energy conservation, while a U processes only need to satisfy energy conservation. Using a fitness criterion of 0.001, the algorithm optimization target is thus to satisfy $D_2 < 0.001$ for U scattering processes and $D_1 + D_2 < 0.001$ for N scattering processes. The N and U scattering processes are treated in two different groups. Phonons engaged in N scattering processes are considered together to satisfy the energy conservation and momentum conservation and phonons engaged in U scattering processes are put together to satisfy the energy conservation. The momentum conservation is not enforced in the calculation for U scattering process, similar to that in Refs. [13–15]. However, simulation results for bulk silicon suggest that neglecting momentum conservation for U process does not significantly affect the simulation result in the temperature range considered in the paper.

As discussed in Ref. [15], in principle, the three-phonon scattering process can be treated by regarding each phonon as a potential candidate for scattering and exploring the possibility of its interaction with every other phonon in its vicinity following the selection rules. That way, the momentum and energy conservations can be met rigorously. However, the computation would be immensely expensive and impossible for most cases. The genetic algorithm provides a way to meet the momentum and energy conservations for N processes and energy conservations for U processes. Compared to the more fundamental approach mentioned above, the genetic algorithm significantly reduces computational time and makes the computation expense acceptable; nevertheless, it is still quite time consuming.

5 N and U Scattering Rates of Phonons

Different expressions for three-phonon scattering rates have been adopted in the literature. Here we choose to use the expressions given by Holland [3]. Even though the phonon scattering rates given by Holland may not be the most physically sound, as discussed in Ref. [22], we choose them here because for bulk Si, extremely good fitting has been achieved with these expressions. In addition, since the most important improvement in the modeling process here from Ref. [15] is the introduction of the genetic algorithm, it is reasonable to keep the Holland scattering rates to see the effect of the genetic algorithm. The N and U scattering rates for transverse and longitudinal acoustic phonons are given as

$$\tau_L^{-1} = B_L \omega^2 T^3 \quad (29)$$

$$\tau_{TN}^{-1} = B_{TN} \omega T^4 \quad (30)$$

$$\tau_{TU}^{-1} = \begin{cases} 0 & (\omega < \omega_{12}) \\ B_{TU} \omega^2 / \sinh\left(\frac{\hbar\omega}{k_B T}\right) & (\omega \geq \omega_{12}) \end{cases} \quad (31)$$

Equation (31) gives the inverse lifetime for longitudinal phonons engaged in the N and U scattering processes. For transverse phonons the U scattering processes do not begin until $\omega \geq \omega_{12}$, where ω_{12} is the transverse branch phonon frequency corresponding to $q/q_{\max} = 0.5$. q_{\max} is the wave vector corresponding to the maximum cutoff frequency of longitudinal phonons in the first Brillouin zone. For bulk Silicon, the maximum cutoff frequency in the longitudinal acoustical branch is 12.3 THz, following the experimental dispersion curve given by Brockhouse [23]. The parameters B_L , B_{TN} , B_{TU} in these equations are listed in Table 1.

When the structure dimension is reduced to the nanoscale, the N and U scattering rates of phonons will be different from that in bulk Si due to confinement effects. The N and U scattering rates in nanowires must be evaluated from first-order perturbation theory based on the phonon dispersion relation for nanowires. The phonon modes in Si nanowires include longitudinal, torsional, and flexural modes. Following the approach used in Ref. [24] to treat cylindrical acoustic waveguides with stress-free boundaries, dispersion relations for these three modes can be obtained from the following equations:

$$(q^2 - q_t^2)^2 \frac{(q_d R) J_0(q_d R)}{J_1(q_d R)} - 2q_d^2 (q^2 + q_t^2) + 4q^2 q_d^2 \frac{(q_t R) J_0(q_t R)}{J_1(q_t R)} = 0 \quad (32)$$

$$q_t R J_0(q_t R) = 2J_1(q_t R) \quad (33)$$

$$J_1(q_d R) J_1^2(q_t R) \phi(q_d, q_t, q, R) = 0 \quad (34)$$

Equation (32) applies to the longitudinal modes, Eq. (33) to the torsional modes, and Eq. (34) to the flexural modes. In all equations q is the z (axial) component of the phonon wave vector, J_0 , J_1 are the ordinary Bessel functions, q_d , q_t are the transverse wave-vector components of dilational and shear waves, and R is radius of the nanowire. Relations between q_d , q_t , and q are

$$q_{q,t}^2 = \frac{\omega^2}{v_{d,t}^2} - q^2 \quad (35)$$

where v_d , v_t are the sound velocities for longitudinal and transverse acoustic waves in bulk Si, respectively. These are given by

$$v_d^2 = (\lambda + 2\mu)/\rho$$

$$v_t^2 = \mu/\rho \quad (36)$$

in which λ , μ are the Lamé constants, and ρ is the density. For bulk Si, the sound velocities are $v_d = 8.47 \times 10^3$ m/s and $v_t = 5.34 \times 10^3$ m/s, respectively. In Eq. (34) the function $\phi = \phi(q_d, q_t, q, R)$ is defined as

$$\phi = f_1 \Psi_\beta^2 + f_2 \Psi_\alpha \Psi_\beta + f_3 \Psi_\beta + f_4 \psi_\alpha + f_5 \quad (37)$$

where

$$f_1 = 2(\beta^2 - \xi^2)^2$$

$$f_2 = 2\beta^2(5\xi^2 + \beta^2)$$

$$f_3 = \beta^6 - 10\beta^4 - 2\beta^4 \xi^2 + 2\beta^2 \xi^2 + \beta^2 \xi^4 + 4\xi^4$$

$$f_4 = 2\beta^2(2\beta^2 \xi^2 - \beta^2 - 9\xi^2) \quad (38)$$

$$f_5 = \beta^2(-\beta^4 + 8\beta^2 - 2\beta^2 \xi^2 + 8\xi^2 - \xi^4)$$

$$\psi_\alpha = \alpha J_0(\alpha)/J_1(\alpha)$$

$$\psi_\beta = \beta J_0(\beta)/J_1(\beta)$$

and

$$\alpha = q_d * R$$

$$\beta = q_t * R \quad (39)$$

$$\xi = q * R$$

For each value of q , the allowed q_t and q_d are found for each phonon branch by selecting the applicable equation from Eqs. (32)–(34) and simultaneously solving with Eq. (35) numerically. The phonon dispersion relations for Si nanowires are then obtained from

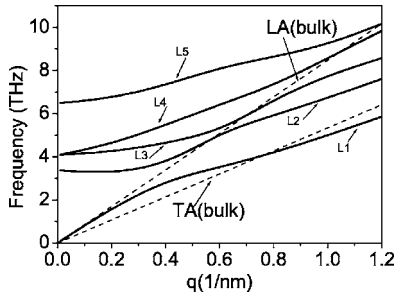


Fig. 1 Longitudinal phonon dispersion relations for 10 nm diameter Si nanowire

$$\omega_n = v_{d,i} \sqrt{q^2 + q_{d,m}^2} \quad (40)$$

where the index n indicates the different allowed branches for a given phonon mode and ω_n is the phonon frequency for the n th branch of that mode.

The calculated dispersion relations for the three phonon modes (longitudinal, flexural, and torsional) are shown in Figs. 1–3, respectively, for a 10 nm diameter Si nanowire. In each mode, the first five branches are given. In Fig. 1, the phonon group velocity of the first longitudinal branch is between the phonon group velocities of longitudinal and transverse acoustic phonons for bulk Si. For small wave vector, the dispersion relation of the first branch of the longitudinal phonon is the same as that of the longitudinal acoustic phonon for bulk Si. As the wave vector increases, the phonon group velocity becomes smaller than that of bulk LA phonon. The first torsional branch is the same as the transverse acoustic phonon for bulk Si. However, the group velocities for other torsional branches and flexural branches are all below the TA mode for bulk Si, which will lead to reduced thermal conductivity. Once the dispersion relation is obtained, the phonon scattering rates can be evaluated according to N and U scattering processes as described below.

It is well known that the momentum of phonons involved in the N process is conserved. The N -scattering process redistributes the

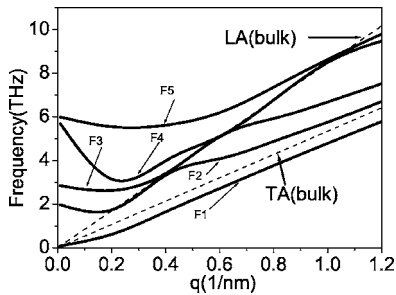


Fig. 2 Flexural phonon dispersion relations for 10 nm diameter Si nanowire

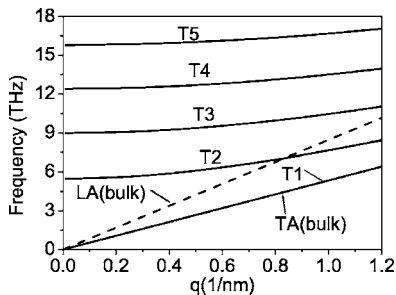


Fig. 3 Torsional phonon dispersion relations for 10 nm diameter Si nanowire

momentum and energy, and prevents strong deviation of each phonon mode from the equilibrium distribution. For N scattering process, there are two mechanisms known as the Herring [25] and Simons mechanisms [26]. The Herring mechanism suggests that the relaxation frequency of the transverse phonons is determined by the three-phonon scattering process involving one transverse and two longitudinal phonons, i.e.,

$$T + L \leftrightarrow L \quad (41)$$

Similar to formula (41), the three-phonon scattering process engaged in nanowire involving the torsional mode (or flexural mode) and two longitudinal modes

$$T + L \leftrightarrow L \quad (42)$$

Equation (42) means that one torsional phonon plus one longitudinal phonons produces one longitudinal phonon or one longitudinal phonon can decay into one transverse phonon and one longitudinal phonon. The scattering rate can be described as

$$\tau_{TN}^{-1} = B_{TN} T^4 \omega_T \quad (43)$$

The relaxation frequency of the longitudinal phonons in the anisotropic continuum system is determined by the three-phonon process according to Simons mechanism [26], whereby either a longitudinal phonon decays into two torsional (flexural) phonons or two torsional phonons combine to form a longitudinal phonon

$$L \leftrightarrow T + T \quad (44)$$

The N scattering rate of the longitudinal phonons can be written as

$$\tau_{NL}^{-1} = B_L T^3 \omega_L^2 \quad (45)$$

The Umklapp process leads to thermal resistance. From the first-order perturbation theory, Klemens [1] gives the relaxation rate for the U process for a thermal or intermediate-frequency state q as

$$\tau_U^{-1} = \frac{2\gamma^2 \hbar}{3\pi^2 \rho v^2 v_g} \omega_i \omega_j (\omega_i + \omega_j) [n(\omega_i) - n(\omega_i + \omega_j)] \int_{q_j} dS' \quad (46)$$

where γ is the Grüneisen parameter, v is the sound velocity, $n(\omega_i)$, $n(\omega_i + \omega_j)$ are the equilibrium occupation of states q_i , $q_i + q_j$. For Si nanowires, the dispersion relations are depicted as in Figs. 1–3. The relaxation rate of U process (46) can be approximated as

$$\tau_U^{-1} = \sum_q \frac{8\gamma^2 \hbar}{3\rho v^2} \omega_i \omega_j (\omega_i + \omega_j) \pi \delta[\Delta\omega]^* [n(\omega_i) - n(\omega_i + \omega_j)] \quad (47)$$

where $\delta[\Delta\omega]$ guarantees that the energy conservation conditions be satisfied, i.e.,

$$\Delta\omega = \omega_i + \omega_j - \omega'' = 0 \quad (48)$$

Eq. (47) describes the relaxation rate of a combining U process, i.e.,

$$\vec{q}_i + \vec{q}_j = \vec{q}'' + \vec{G} \quad (49)$$

where \vec{G} is the shortest reciprocal-lattice vector. q_i , q_j are the interacting states with high frequency near the zone boundary. $v_g = \|\partial\omega(q'')/\partial q''\|$ is the group velocity at $\omega'' = \omega_i + \omega_j$ in the longitudinal mode in the principal direction. The factor $\int_{q_j} dS'$ is the area of the momentum space of the interacting state q_j with the reference state q_i . In order to obtain the scattering rate for the U process at state of q_i , all of the possible interacting channels must be taken into account, then sum those scattering rates together. However, at temperatures lower than the Debye temperature, the lowest order branches are the most important branches. In order to

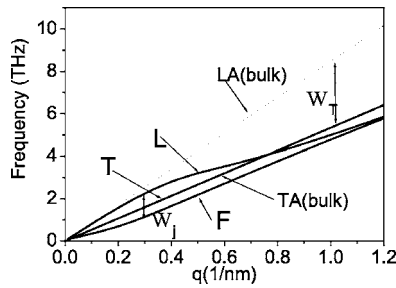


Fig. 4 Dispersion relation for the lowest longitudinal, flexural, and torsional branches of a 10 nm diameter Si nanowire

demonstrate the calculation procedure, only the first branches for each of the three modes are taken into account as shown in Fig. 4. This approximation neglects the populated phonons at higher energy level in the quasi-optical branches. However, as shown in Figs. 1–3, the lowest branches in each mode have the highest phonon group velocities. Compared with previous work [27,31], this approximation will overestimate the energy transport at low temperatures. Based on the Klemens two-step model [28], Eq. (46) can be simplified as [31]

$$\tau_U^{-1} = \frac{2\gamma^2\hbar}{3\pi\rho v^2 v_g} \omega_i \omega_j (\omega_i + \omega_j) r_c^2 \exp(-\hbar\omega_j/k_B T) \quad (50)$$

where

$$\int_{q_j} dS' = \pi r_c^2, r_c = R_c [G/2 - q_i] / (G/2), R_c = \pi / (\sqrt{2}a) \quad (51)$$

Here ω_j is the frequency gap between the two different modes as shown in Fig. 4. The relaxation rate for bulk Si can be obtained in the same procedure and the ratio between the two time scales can be obtained approximately as

$$\frac{\tau_U^{-1, \text{nano}}}{\tau_U^{-1, \text{bulk}}} \propto \frac{v_g^{\text{bulk}}}{v_g^{\text{nano}}} \exp[\hbar(\omega_T - \omega_j)/k_B T] \quad (52)$$

where ω_T is the frequency gap between the longitudinal and transverse modes in bulk Si phonon dispersions as shown in Fig. 4. The superscripts bulk and nano stand for bulk material and nanowires in Eq. (52). Equation (52) demonstrates that the Umklapp scattering rate of nanowires is inversely proportional to the phonon group velocity and the frequency gap between different branches in the nanowire. With decreasing phonon group velocity and frequency gap between different modes, the Umklapp scattering rate increases greatly compared with the phonons scattering rate in bulk material.

6 Numerical Results

The phonon transport in single Si nanowires was simulated using MC. Impurity scattering was neglected in the current simulation since our primary interest in this paper is thermal conductivity at high temperatures, where impurity scattering is not as significant. Additionally, in nanowires the boundary scattering is usually strong enough to mask the impurity scattering. The cross section of the nanowires is square with side length a . It is assumed that the dispersion relations developed above for cylindrical waveguides are applicable here when $2R=a$. The main reason for this is that we have a closed form expression for the dispersion of round wires, which is easier to be included in the simulation. We believe that this is acceptable because if we do not consider the dispersion relation modification due to confinement, the boundary simply provides boundary scattering, which limits the phonon mean free path to be on the order of the wire diameter depending on the selection of the specularly parameter. The real shape of the nanowire in our simulation does not affect the simulation results.

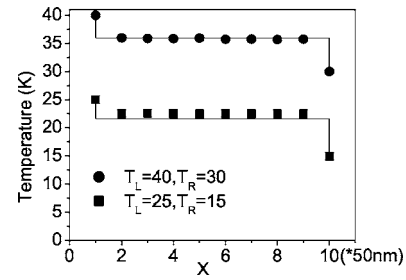


Fig. 5 "Temperature" distribution along the Si nanowire under ballistic transport condition. T_L , T_R correspond to the temperatures on the left and right ends of the nanowire.

In order to verify that the MC model correctly predicts phonon transport, we first chose a simple problem: ballistic phonon transport between the two ends of the nanowire. Ballistic transport becomes important at low temperatures, where U processes are frozen out and impurity and boundary scattering are negligible. In this situation there is no thermal resistance and the "temperature" remains constant along the sample length [13]

$$T^4 = (T_L^4 + T_R^4)/2 \quad (53)$$

Here T_L , T_R stand for the temperatures at the two ends of the nanowire. The ballistic condition was realized in the MC simulations by neglecting all scattering processes. The results from both theoretical solution, Eq. (53), and the simulations of a Si nanowire with a total length of 500 nm and $a=50$ nm are shown in Fig. 5 for two different temperatures. The nanowire was divided into ten cells along its length and the local "temperature" in each cell was obtained by fitting the distribution to the Bose-Einstein distribution. Strictly speaking, temperature can only be defined in each cell when local thermodynamic equilibrium is reached, which is clearly not true for the ballistic case. For long enough simulations, however, the hot and cold phonons traveling in opposite directions are sufficiently averaged so that the numerical results in Fig. 5 (symbols) agree well with the theory (line).

Bulk Si was also simulated to further verify the model. This was done by setting the specularly parameter $d=1$, which means that the nanowire surfaces are perfectly smooth and all the phonons are specularly reflected. Since boundary scattering does not contribute to thermal resistance in this case, the nanowire MC model using the bulk Si phonon dispersion relation should yield thermal conductivity values close to that of bulk Si at high temperatures. However, at low temperature, the simulation results deviate from the experimental value due to the lack of boundary and impurity scattering.

Figure 6 illustrates that this is indeed the case: The MC numerical results circles for a nanowire with $d=1$ agree well with the experimental results for bulk Si [3] for temperatures greater than 25 K. The simulation results also agree well with recently reported experimental data on enriched isotope silicon [22,29]. For tem-

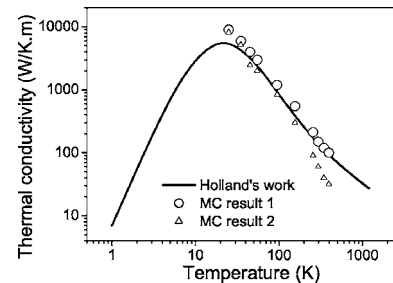


Fig. 6 Temperature dependence of bulk Si thermal conductivity from MC simulation results

peratures below 25 K, the thermal conductivity of bulk Si is dominated by phonon-boundary scattering, and the numerical results (not shown) approach infinity.

In order to demonstrate the advantage of the generic algorithm, we applied the MC code to bulk Si without the genetic algorithm. In this case, the momentum conservation of the N scattering processes is removed, and the MC code is the same as that in Ref. [15]. The simulation results are also shown in Fig. 6 as the triangle marks. It is clear that without the conservation of momentum for N processes, the simulation results give much lower values at high temperature. This is because without conservation of momentum, the N process directly poses resistance to thermal transport since only energy conservation is satisfied. It is well known that the N process only contributes to the thermal resistance indirectly by redistributing the phonons and restoring the equilibrium distribution. So without a physically sound modeling of the N process, the results deviate from the experimental value for bulk Si.

During the simulation process, it is observed that the length scale of the simulation domain may have an artificial effect on the final simulation results over the temperature range from 25 K to 500 K. Especially at low temperatures, since the scale of the simulation domain may be smaller than the phonon mean free path, temperature jumps appear between the ends of the simulation cell and the boundary walls. At high temperatures, the size of the simulation domain is usually larger than the phonon mean path. In this case, a nonlinear temperature profile arises due to the temperature dependence of thermal conductivity. In order to get precise simulation results, two criteria should be satisfied: The effective thermal flux in each simulation cell should be nearly the same, and the temperature profiles should be reasonably close to linear. The profiles should not be expected to be completely linear, since the thermal conductivity is temperature dependent. In order to satisfy the two criteria, computation time should be selected to be as long as possible for the system to reach steady state. In this paper, to avoid undue computational burden, values roughly 20 times of the characteristic diffusion time were found sufficient to satisfy the criteria. Time step is another factor affecting the simulation results. It should be smaller than the smallest scattering time scale to avoid missing a scattering process. Considering that different simulation cell sizes and different temperatures are used, the time step can be chosen based on the approximation that during each time step, the distance traveled by the fastest phonons is about one fourth the simulation cell. The choice of the simulation domain size at different temperatures is also a formidable task. The length of the simulation domain should be larger than the longest phonon free path to completely remove the temperature jump at the two ends. However, it is difficult to determine the mean free path for each phonon. A trial-and-error process was thus used to find the length scale of the simulation domain. For a certain simulated temperature, the length of the simulated nanowire should meet the demands that the temperature profile remains linear and no temperature jumps appear in the two ends. For the thermal conductivity simulations reported here, the values of the effective thermal flux in each cell were all within ten percent of the averaged flux and the temperature profiles were essentially linear. Finally, in order to further reduce noise effects on the final simulation results, three different simulation runs were averaged that differed only by the seed value used in the simulation's random number generator. Error analysis shows the difference between the three simulation runs are within five percent.

Figure 7 shows calculated and experimental thermal conductivities of Si nanowires of diameters 115 nm, 37 nm, and 22 nm. The three solid lines represent MC simulation results calculated using the dispersion relation for bulk Si, and the symbols represent experimental results from Ref. [16]. In the MC simulation procedure, the impurity scattering and the boundary scattering are all considered. The specular parameter was calibrated to fit the simulation result to the experimental data [16]. Its value was set to

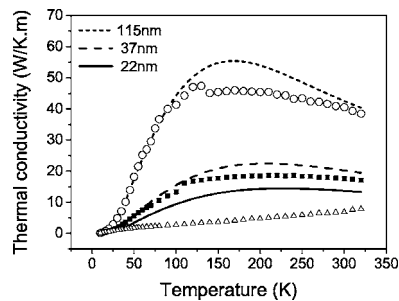


Fig. 7 Thermal conductivity of Si nanowires with different diameters: MC simulation with bulk dispersion relation (lines) and experiment (symbols)

0.5 based on several round tried simulations. The impurity scattering parameter B_i , as shown in Table 1, was obtained using a similar procedure. The parameters B_N and B_U were assumed the same as those for bulk silicon. The MC simulation results agree reasonably well with the experimental results for nanowires with diameters 37 nm and 115 nm. The position for the peak value of thermal conductivity for Si nanowires is displaced to higher temperature compared with that for bulk Si, which is 25 K. This is because for nanowires, boundary scattering is the dominant phonon scattering mechanism up to much higher temperatures.

Quite a few theoretical studies on the thermal transport in nanowires have been reported [30–37]. Several of them [30–34] are theoretical investigations working on hypothetical model system without comparison to experimental results. Those studies are trying to disclose the effects of diffuse/specular boundary reflections, ballistic/diffuse transport and scattering rate change due to phonon dispersion changes in nanowires. More recent theoretical studies [35–37] compared their modeling results with the experimental data [16]. The theoretical results from those studies match the experimental data reasonably well, similar to the present work, for nanowires with diameters larger than 37 nm. Most of the studies in the literature are based on closed form integration, which is not as computationally expensive as the present study. However, Monte Carlo simulation provides a more rigorous approach to the phonon transport and has the potential to be applied to complex geometry.

For the 22 nm diameter wire, the difference between the MC simulation and the experimental results is significant. As discussed above, the phonon dispersion relation at this length scale can differ significantly from that of the bulk and may be the reason for the difference. In order to see if this is the case, the nanowire phonon dispersion relations were used instead of bulk phonon dispersion relations in the MC model. Phonon transport in different diameter nanowires was simulated with different dispersion relations at 300 K (Fig. 8). In Fig. 8, model 1 refers to results obtained using nanowire phonon dispersion and model 2 refers to results obtained using bulk silicon phonon dispersion relations. It

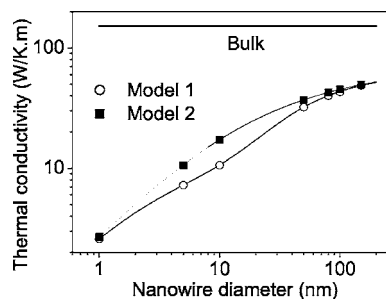


Fig. 8 Nanowire thermal conductivity versus diameter at $T = 300$ K

can be seen from the figure that for large diameter nanowires, the results from different dispersion relations are nearly the same. However, as the nanowire diameter decreases, the difference gets larger and can be observed clearly. The thermal conductivity evaluated from nanowire dispersion relations become significantly smaller than that from the dispersion relation for bulk Si. The maximum difference occurs for nanowires with a diameter between 10 nm to 20 nm. For even smaller diameter nanowires, the difference gets smaller. The reason for this is not fully understood. However, we believe that in this case the strong boundary scattering will prohibit phonon transport and dominate over any other scattering events. This reduces thermal conductivities calculated using both bulk and nanowire dispersion relations to nearly the same value. The reason for smaller thermal conductivity from nanowire dispersion relations may be from two sources. One is that the phonon group velocity in nanowires is smaller than that in bulk material. The other is that the phonon lifetime evaluated from Eq. (47) is smaller than that obtained from the formula for bulk material. With decreasing nanowire diameter, the frequency gap between different branches decreases, which in turn causes the increase of phonon Umklapp scattering rate, and hence reduces the lattice thermal conductivity. Since simulations using nanowire dispersion relations are very time consuming, a detailed calculation for the thermal conductivity of different diameter nanowires spanning a broad temperature range has not yet been carried out.

7 Conclusion

A Monte Carlo method has been developed to simulate phonon transport in nanowires. A genetic algorithm, which meets both momentum and energy conservation requirements for the simulation system, was adopted to model the phonon-phonon scattering process. Phonon dispersion relations for bulk Si and Si nanowires were employed to simulate nanowire thermal conductivity. Simulation results using the bulk Si dispersion relation agree reasonably well with our experimental results for nanowires with a diameter larger than 37 nm. Simulation results using the nanowire dispersions show significant differences compared with those using the bulk dispersions for nanowires with a diameter between 10 nm and 20 nm. These differences were attributed to the phonon group velocity reduction and the phonon lifetime reduction due to strong phonon-phonon scattering derived from nanowire dispersion relations.

Acknowledgments

Y. Chen would like to acknowledge the financial support from the National Natural Science Foundation of China (5027601, 50275026) and the 863 High Technology Program (2003AA404160). The authors would also like to thank Dr. Sandip Mazumder of CFD Research Corporation for the helpful discussions about the MC algorithm.

References

- [1] Klemens, P. G., 1958, *Solid State Physics*, Academic Press, NY.
- [2] Callaway, J., 1959, "Model of Lattice Thermal Conductivity at Low Temperatures," *Phys. Rev.*, **113**, pp. 1046–1051.
- [3] Holland, M. G., 1963, "Analysis of Lattice Thermal Conductivity," *Phys. Rev.*, **132**, pp. 2461–2471.
- [4] Armstrong, B. H., 1985, "N Processes, the Relaxation-Time Approximation, and the Thermal Conductivity," *Phys. Rev. B*, **32**, pp. 3381–3390.
- [5] Chen, G., 2001, "Ballistic-Diffusive Heat-Conduction Equations," *Phys. Rev. Lett.*, **86**, pp. 2297–2230.

- [6] Ju, Y. S., and Goodson, K. E., 1999, "Phonon Scattering in Silicon Thin Films with Thickness of Order 100 nm," *Appl. Phys. Lett.*, **14**, pp. 3005–3007.
- [7] Kurosawa, T., 1966, "Monte Carlo simulation of hot electron problems," *Proceedings of the International Conference on the Physics of Semiconductor*, Kyoto, J. Phys. Soc. Jpn. **21**, pp. 424–427.
- [8] Budd, H., 1967, "Path Variable Formulation of the Hot Carrier Problem," *Phys. Rev.*, **158**, pp. 798–804.
- [9] Jacoboni, C., and Reggiani, L., 1983, "The Monte Carlo Method for the Solution of Charge Transport in Semiconductors with Applications to Covalent Materials," *Rev. Mod. Phys.*, **55**, pp. 645–705.
- [10] Bachelier, L., and Jacoboni, C., 1972, "Electron-Electron Interactions in Monte Carlo Transport Calculations," *Solid State Commun.*, **10**, pp. 71–74.
- [11] Matulionis, A., Pozela, J., and Reklaitis, A., 1975, "Monte Carlo Treatment of Electron-Electron Collisions," *Solid State Commun.*, **16**, pp. 1133–1137.
- [12] Jacoboni, C., 1978, "Noise and Diffusion of Hot Holes in Si," *Solid-State Electron.*, **21**, pp. 315–318.
- [13] Klitsner, T., VanCleve, J. E., Fisher, H. E., and Pohl, R. O., 1988, "Phonon Radiative Heat Transfer and Surface Scattering," *Phys. Rev. B*, **38**, pp. 7576–7594.
- [14] Peterson, R. B., 1994, "Direct Simulation of Phonon-Mediate Heat Transfer in A Debye Crystal," *ASME J. Heat Transfer*, **116**, pp. 815–822.
- [15] Mazumder, S., and Majumdar, A., 2001, "Monte Carlo Study of Phonon Transport in Solid Thin Films including Dispersion and Polarization," *ASME J. Heat Transfer*, **123**, pp. 749–759.
- [16] Li, D., Wu, Y., Kim, P., Shi, L., Yang, P., and Majumdar, A., 2003, "Thermal Conductivity of Individual Silicon Nanowires," *Appl. Phys. Lett.*, **83**, pp. 2934–2936.
- [17] Li, D., Wu, Y., Fan, R., Yang, P., and Majumdar, A., 2003, "Thermal Conductivity of Si/SiGe Superlattice Nanowires," *Appl. Phys. Lett.*, **83**, pp. 3186–3188.
- [18] Vincenti, W. G., and Kruger, C. H., 1977, *Introduction to Physical Gas Dynamics*, Robert Krieger Publication, New York.
- [19] Majumdar, A., 1993, "Microscale Heat Conduction in Dielectric Thin Films," *ASME J. Heat Transfer*, **115**, pp. 7–16.
- [20] Peierls, R. E., 1955, *Quantum Theory of Solids*, Oxford University Press, Oxford.
- [21] Goldberg, D. E., 1982, *Genetic Algorithms in Search, Optimization, and Machine Learning*, Addison-Wesley Publishing Company.
- [22] Asen-Palmer, M., Bartkowski, K., Gmelin, E., Cardona, M., Zhernov, A. P., Inyushkin, A. V., Taldenkov, A., Ozhogin, V. I., Itoh, K. M., and Haller, E. E., 1997, "Thermal Conductivity of Germanium Crystals with Different Isotopic Compositions," *Phys. Rev. B*, **56**, pp. 9431–9447.
- [23] Brockhouse, B. N., 1959, "Lattice Vibrations in Silicon and Germanium," *Phys. Rev. Lett.*, **2**, pp. 256–258.
- [24] Auld, B. A., 1973, *Acoustic Fields and Waves in Solids*, Wiley, NY.
- [25] Herring, C., 1954, "Role of Low Energy Phonons in Thermal Conduction," *Phys. Rev.*, **95**, pp. 954–965.
- [26] Simons, S., 1963, *Proc. Phys. Soc. London*, **82**, pp. 401–405.
- [27] Blencowe, M. P., 1999, "Quantum Energy Flow in Mesoscopic Dielectric Structures," *Phys. Rev. B*, **59**, pp. 4992–4998.
- [28] Han, Y.-J., and Klemens, P. G., 1993, "Anharmonic Thermal Resistivity of Dielectric Crystals at Low Temperatures," *Phys. Rev. B*, **48**, pp. 6033–6042.
- [29] Kremer, R. K., Graf, K., Cardona, M., Devyatikh, G. G., Gusev, A. V., Gibin, A. M., Inyushkin, A. V., Taldenkov, A. N., and Pohl, H.-J., 2004, "Thermal Conductivity of Isotopically Enriched 28Si: Revisited," *Solid State Commun.*, **131**, pp. 499–503.
- [30] Zou, J., and Alexander, B., 2001, "Phonon Heat Conduction in A Semiconductor Nanowire," *J. Appl. Phys.*, **89**, pp. 2932–2938.
- [31] Khitun, A., and Wang, K. L., 2001, "Modification of the Three-Phonon Umklapp Process in A Quantum Wire," *Appl. Phys. Lett.*, **79**, pp. 851–853.
- [32] Volz, S., Lemonnier, D., and Saulnier, J.-B., 2001, "Clamped Nanowire Thermal Conductivity Based on Phonon Transport Equation," *Microscale Thermophys. Eng.*, **5**, pp. 191–207.
- [33] Lü, X., Chu, J. H., and Shen, W. Z., 2003, "Modification of the Lattice Thermal Conductivity in Semiconductor Rectangular Nanowires," *J. Appl. Phys.*, **93**, pp. 1219–1229.
- [34] Volz, S., and Chen, G., 1999, "Molecular Dynamics Simulation of Thermal Conductivity of Silicon Nanowires," *Appl. Phys. Lett.*, **75**, pp. 2056–2058.
- [35] Dames, C., and Chen, G., 2004, "Theoretical Phonon Thermal Conductivity of Si/Ge Superlattice Nanowires," *J. Appl. Phys.*, **95**, pp. 682–693.
- [36] Mingo, N., 2003, "Calculation of Si Nanowire Thermal Conductivity using Complete Phonon Dispersion Relations," *Phys. Rev. B*, **68**, pp. 113308–113308-4.
- [37] Mingo, N., Yang, L., Li, D., and Majumdar, A., 2003, "Predicting the Thermal Conductivity of Si and Ge Nanowires," *Nano Lett.*, **3**, pp. 1713–1716.